

Si membrane based tactile sensor with active matrix circuitry for artificial skin applications

Minhoon Park, Min-Seok Kim, Yon-Kyu Park, and Jong-Hyun Ahn

Citation: [Applied Physics Letters](#) **106**, 043502 (2015); doi: 10.1063/1.4906373

View online: <http://dx.doi.org/10.1063/1.4906373>

View Table of Contents: <http://scitation.aip.org/content/aip/journal/apl/106/4?ver=pdfcov>

Published by the [AIP Publishing](#)

Articles you may be interested in

[Design and fabrication of a CMOS-compatible MHP gas sensor](#)

AIP Advances **4**, 031339 (2014); 10.1063/1.4869616

[Extremely robust and conformable capacitive pressure sensors based on flexible polyurethane foams and stretchable metallization](#)

Appl. Phys. Lett. **103**, 204103 (2013); 10.1063/1.4832416

[Steady heat conduction-based thermal conductivity measurement of single walled carbon nanotubes thin film using a micropipette thermal sensor](#)

Rev. Sci. Instrum. **84**, 034901 (2013); 10.1063/1.4792841

[Nanostructured anatase-titanium dioxide based platform for application to microfluidics cholesterol biosensor](#)

Appl. Phys. Lett. **101**, 084105 (2012); 10.1063/1.4747714

[Flexible ferroelectret field-effect transistor for large-area sensor skins and microphones](#)

Appl. Phys. Lett. **89**, 073501 (2006); 10.1063/1.2335838

A banner for Applied Physics Letters featuring the journal's logo and the text 'Meet The New Deputy Editors'. Below the text are three circular headshots of the new deputy editors: Alexander A. Balandin, Qing Hu, and David L. Price.

AIP | Applied Physics Letters

Meet The New Deputy Editors

 Alexander A. Balandin

 Qing Hu

 David L. Price

Si membrane based tactile sensor with active matrix circuitry for artificial skin applications

Minhoon Park,^{1,2} Min-Seok Kim,^{2,a)} Yon-Kyu Park,² and Jong-Hyun Ahn^{1,a)}

¹*School of Electrical and Electronic Engineering, Yonsei University, Seoul 120-749, South Korea*

²*Center for Mass Related Quantities, Korea Research Institute of Standards and Science, Daejeon 305-340, South Korea*

(Received 13 September 2014; accepted 6 January 2015; published online 29 January 2015)

The fabrication and the characteristics of an inorganic silicon-based flexible tactile sensor equipped with active-matrix circuitry compatible with a batch microfabrication process are reported. An 8×8 array of 260 nm-thick silicon strain gauges along with individual thin film transistor switches was built on a plastic substrate with 1 mm spacing, corresponding to a human spatial resolution at the fingertip. We demonstrated that the sensor shows excellent performances in terms of repeatability of 1.1%, hysteresis of 1.0%, scanning speed of as much as 100 kHz and resolution of 12.4 kPa while maintaining low power consumption and signal crosstalk through a series of experiments.

© 2015 AIP Publishing LLC. [<http://dx.doi.org/10.1063/1.4906373>]

For biomedical and robotic applications, the development of highly malleable, user-interactive electronic skin with tactile sensing capabilities is in high demands as it is one of the critical technologies. Like the human skin, the tactile sensor should provide robust, reliable, and fast feedback of force distribution including its contact shape and location as well as enough mechanical flexibility and elasticity, while preserving its original properties under high external strain. A considerable amount of research to improve the sensitivity and mechanical property of tactile sensors has been carried out.^{1–3} One representative approach is to use the piezoresistive polymer composite, comprised conductive materials (mostly in particle type) and elastic rubber matrixes. Despite promising mechanical properties of the composite, its inconsistent repeatability, poor stability, high non-linearity, and high hysteresis limit the range of its applications.⁴ The approach using resistance change of strain gauges or capacitance change of dielectric material between two conductive plates, deformed under pressure, could circumvent these problems. Compared to the capacitance measurements, the readout circuitry for the resistance measurements is straightforward and simple. This makes it much easier to implement so-called “on-board signal processing” (i.e., the readout circuitry integrated with sensors), which is one of critical requirements for accommodating large number of sensing elements in the limited available space like a robot finger.^{5,6}

We employed the approach using resistance change of strain gauges made of single-crystal silicon (Si) to develop a flexible, high-performance, and highly integrated tactile sensing array. The use of single-crystal Si incorporates both benefits of high-sensitivity originated from a high gauge factor (GF) of semiconductor strain gauges measured to be 50–150 compared to that of metallic strain gauges of 2–3 and high-performances, such as high switching speed and on/off ratio resulting from a high mobility and moderate band-gap energy of inorganic Si compared to those of

organic materials. In addition to such benefits, the sensing array and its corresponding readout circuitry could be fabricated together and integrated in one substrate through a batch micromachining process. Recent research directed towards the fabrication of ultrathin Si-nanomembrane (NM) through etching and transfer processes permits a mechanically flexible and robust Si device, which leads to the demonstration of various Si NM-based flexible sensors and actuators worn on finger tips.^{7,8} Nevertheless, significant challenge still remains in the integration of these Si NM-sensors to active-matrix thin film transistors (TFTs) capable of acting as a switch for both current-driven and voltage-driven devices in order to multiplex the sensor array with low crosstalk among sensing elements and high switching speed.

Now we report a design, fabrication methods, and performances of a Si NM-based flexible tactile sensor equipped with basic on-board signal processing circuitry consisting of a TFT switch array for multiplexing. In particular, a Si-NM sheet was transfer-printed on a plastic substrate, and then the Si strain gauges and the Si-semiconducting channels were monolithically integrated by the conventional CMOS process. A series of experiments demonstrated that the developed tactile sensor array with active-matrix back plane circuitry displays faster response and better spatial contrast resulting from a decrease in signal crosstalk along with good sensor output characteristics in terms of repeatability, hysteresis, and sensitivity.

Figure 1 illustrates the steps for fabricating the flexible tactile sensor consisting of an 8×8 array of silicon strain gauges and readout TFTs integrated into the area of 10 mm^2 (approximately corresponding to the area of fingertips) using a single-crystal Si NM. First, an adequate doping step was applied to the Si NM on silicon-on-insulator (SOI) wafer in order to create p-type semiconductor strain gauge region and n-type the source and drain region of transistors through two separate processes of boron and phosphorus implantation with a concentration of $9.0 \times 10^{18} \text{ ions/cm}^3$ and $1.0 \times 10^{19} \text{ ions/cm}^3$, respectively. The top silicon (260 nm thick) was transferred to a polyimide substrate ($25 \mu\text{m}$) using a polydimethylsiloxane

^{a)}Authors to whom correspondence should be addressed. Electronic addresses: mink@kriss.re.kr and ahnj@yonsei.ac.kr

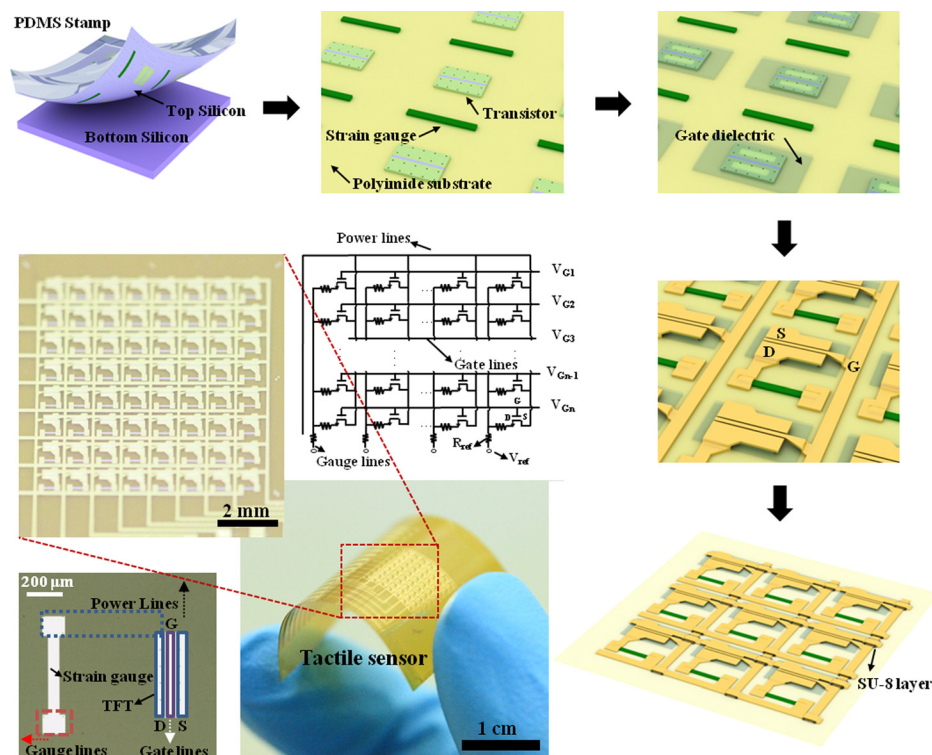


FIG. 1. Illustration of the tactile sensor. The dry transfer method was used to fabricate the device in a low temperature. The transferred gauges and the transistors were shaped in such a way to include the isolation process, gate dielectric deposition, 1st metallization, SU-8 passivation, and 2nd metallization. This device was built on the polyimide substrate ($25 \mu\text{m}$) to achieve mechanical flexibility. The inset on the bottom left gives an optical image of a unit cell consisting of a strain gauge and a transistor. The inset on the center shows the electrical circuit including the resistance, electrode lines, and transistors. See Fig. S1 in supplementary material²⁴ for the detailed optical images at each fabrication step.

(PDMS) stamp after a wet etching of the buried SiO_2 layer. The overall transfer yield was close to 100%. The reactive-ion etching (RIE) was used to remove the undoped region of the top silicon layer and shape strain gauges and transistors, followed by PECVD (Plasma enhanced chemical vapor deposition) to create a SiO_2 dielectric layer selectively on the Si channel region of readout transistors. Finally, a metal (Cr/Au: 5/200 nm) layer was deposited by thermal evaporation and etched to shape electrodes and electrical lines.

The sensor array includes the switching transistors for data readout, the strain gauges for pressure sensing, and the electrical lines (the center inset of Figure 1). All transistors in a same row (total 8 transistors) are turned on simultaneously when a voltage for on-states is applied to the corresponding gate line and an external analogue-digital converter with 8 channels reads the resistance of all strain gauges in the turned-on gate line at the same time via the voltage measurements at voltage dividers consisting of reference resistors. Multiplexing gate lines and gathering resistance changes of the strain gauges in the selected gate line sequentially create a pressure map with time for visualization. The tactile sensor with active-matrix circuitry made electrical wiring much simpler, enabling us to integrate 64 strain sensors within an area of smaller than 10 mm^2 , corresponding to the area of a human fingertip.

Figures 2(a) and 2(b) present DC characteristics of the single-crystal Si-based switching transistor. The single-crystal Si transistor shows an on/off ratio of greater than 10^6 , a field effect mobility, μ_{FE} , of $661 \text{ cm}^2/\text{V}\cdot\text{s}$, and a threshold voltage of 0.5 V. It also provided a stable current flow even at a high switching frequency of 100 kHz with negligible noise during a pulse measurement test. These features enable us to provide a real-time tactile feedback by multiplexing sensing elements via a sequential high-speed TFT switching operation^{9–12} that cannot be easily achieved by using

organic-based transistors due to their relatively poor carrier mobility or using the highly semiconductor-enriched single-wall nanotube (SWNT) transistors due to their material non-uniformity.^{13,14} In addition to such complementary features, the strain sensor is also a factor in the performance of the tactile sensor array. PSR (pressure sensitive rubber) materials, generally used in flexible tactile sensors, carry the intrinsic limitation of resolution due to their anisotropic

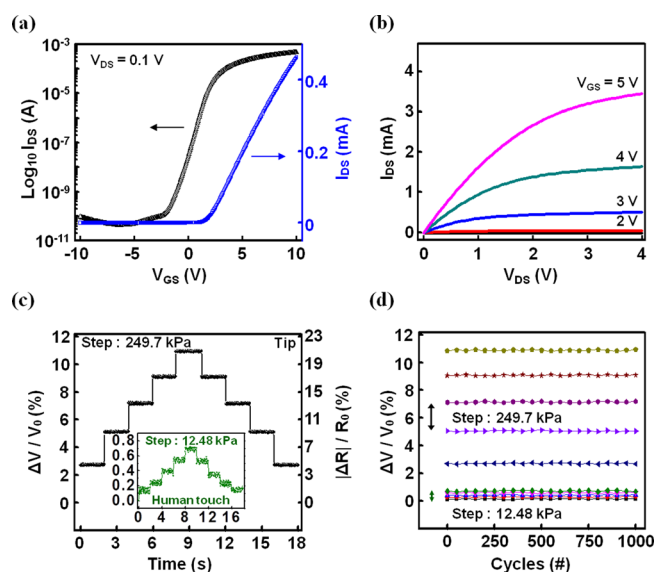


FIG. 2. (a) The transfer characteristic of drain-to-source current from a transistor in logarithmic (left y-axis) and linear (right y-axis) scales as gate to source voltage (V_{GS}) was swept from -10 V to $+10 \text{ V}$. (b) I-V curve of the switching transistor at gate voltages from 0 V (bottom) to 5 V (top) in 1 V steps. (c) The characteristic curve as a function of time at various pressure levels with 249.7 kPa steps. The inset on bottom center shows the properties in a low range of pressure levels with 12.48 kPa steps. (d) The variation of the output of a single tactile unit for the repeatable loads (cycles up to 1000) with various pressure levels from 0 kPa to 1248 kPa .

characteristic between vertical and horizontal conductivity as well as problems of high hysteresis and poor repeatability as mentioned previously.^{15–18} Compared to PSR materials, Si-based strain gauges show good characteristics in terms of linearity, hysteresis, repeatability, and sensitivity originated from a high gauge factor of semiconducting materials as a function of external strain or pressure. The GF of our device was theoretically calculated to be 85.5 using Eq. (1),¹⁹ which is approximately 40 times higher than that of conventional metallic strain gauges

$$GF = 1 + 2\lambda + Y \times P(N, T) \times \pi(300 \text{ K}), \quad (1)$$

where the Poisson's ratio λ , the young's modulus Y , piezoresistance factor $P(N, T)$, and the piezoresistance coefficient π are assumed to be 0.05, 168 GPa, 0.7, and $71.8 \times 10^{-11} \text{ Pa}^{-1}$, respectively, at the doping concentration N of $9.0 \times 10^{18} \text{ cm}^{-3}$ and temperature T of 300 K. This theoretical estimation of the gauge factor agrees with the one determined experimentally to be 86.1 by measuring a change in the fractional resistance ($\Delta R/R_0$) and the corresponding strain under maximum pressure at flat state (see Fig. S2 in supplementary material²⁴).

Fig. 2(c) shows the output characteristics of a Si-strain gauge as a function of pressure and time. The inset presents the characteristics in a low pressure range, and the minimum distinguishable pressure (12.4 kPa) is comparable to the threshold values of human skin in a range of 10–40 kPa.²⁰ Curves of the fractional change in output voltage ($\Delta V/V_0$) at various pressure levels with 12.48 and 249.7 kPa steps show that the Si-based tactile sensor has low hysteresis, low creep (i.e., drift with time) [Fig. 2(c)], and low repeatable error [Fig. 2(d)], which are determined to be maximum 1.0%, 0.5%, and 1.1% among 1000 cycle data for each pressure level.

Our sensor was designed from the perspective of human skin that has the receptors to measure physical quantities. These receptors are embedded in a viscoelastic dermis to protect themselves from the external environment. Similarly, both sides of our Si-based sensor array are covered with viscoelastic PDMS substrates of same thickness of 1 mm to protect the sensing elements (Fig. S3 in supplementary material²⁴). This structure could also improve the bending radius of the sensor array on a substrate by making the position of the Si-devices close to the neutral mechanical plane. As the top protective PDMS cover gets thinner, the sensitivity could get better, which is improved approximately by a factor of 2 when the thickness of the top PDMS substrate is reduced to 0.7 mm. However, we have observed a malfunction of TFT arrays due to a high strain when the thickness of the top protective layer gets smaller than 0.7 mm. Figure 3(a) presents a variation in the fractional voltage change, $\Delta V/V_0$, with various bending radius changed from 10 mm to infinity (i.e., flat). The variation was measured to be only 5% due to such elastomer passivation. Fig. 3(b) shows a change in normalized mobility, $\mu_{\text{eff}}/\mu_{0\text{eff}}$, during the pressure test of the single-crystalline transistor at various bending radii, where $\mu_{0\text{eff}}$ is a mobility value measured at zero pressure and flat state. The variations due to the bend radius change and pressure were measured to be small enough (less than 10%) not to deteriorate original performances of the TFTs that are

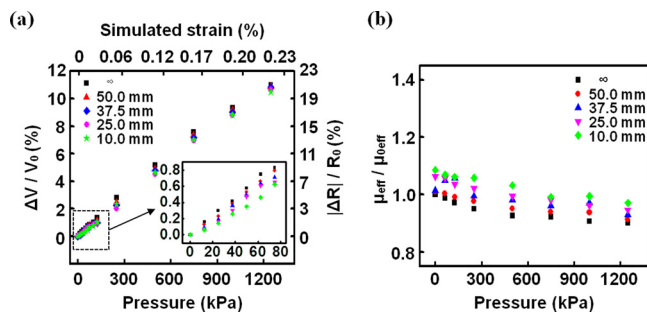


FIG. 3. (a) The fractional change in output voltage as a function of pressure and strain measured at various bending radii. The inset on the right bottom presents the results at low levels of pressure. (b) The normalized effective mobility as a function of pressure measured at various bending radii.

required to run active matrix circuitry properly even at a bending radius corresponding to the curvature of the human finger.

Since the tactile sensor is required to provide prompt and reliable data acquisition even on curved surfaces, the Si-based sensor array was tested while being attached on the finger. Figure 4(a) shows the optical image of the tactile sensor attached on the fingertip. The tactile sensor could discriminate two contact points spaced 1 mm, corresponding to a spatial resolution of the human skin, as shown in the inset (top left) of Fig. 4(b). When one tactile cell was touched by a small tip whose size corresponds to that of the strain gauge (radius: 0.125 mm), the voltage output only at the corresponding cell was noticeably increased, whereas the voltage changes of other adjacent tactile cells were measured to be negligibly low (i.e., low crosstalk among tactile cells) during multiplexing operation, as shown in the inset (top right) of Fig. 4(b). This is due to the high on/off ratio of the Si-based TFTs that controls the current flow of each tactile cell. The crosstalk isolation, which is defined as Eq. (2), was measured to be an average of 37.2 dB and the maximum value of 42.0 dB during the touch test. The crosstalk isolation is given by

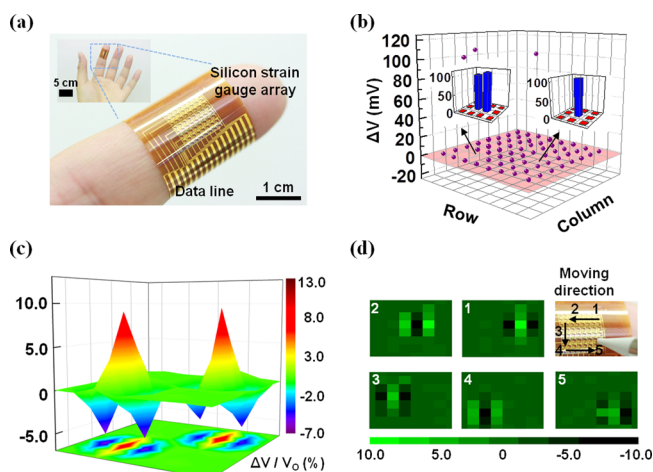


FIG. 4. (a) The tactile sensor attached to a human fingertip. It consists of an 8×8 array of Si strain gauges and Si TFTs. (b) The voltage output of the tactile sensor in response to localized pressure inputs showing its low crosstalk and spatial resolution. (c) A pressure distribution map acquired during the multi-touch test. (d) A series of 5 frames of the tactile image showing tracking the position of a stylus tip moving fast on the sensing array. The data acquisition electronic system grabbed each frame of the tactile image every 10 ms. Only 5 frames are shown among the acquired frames.

$$(\text{The crosstalk isolation}) = 20 \log_{10} \left(\frac{\Delta V_{\text{applied cell}}}{\Delta V_{\text{adjacent cell}}} \right), \quad (2)$$

where $\Delta V_{\text{applied cell}}$ and $\Delta V_{\text{adjacent cell}}$ represent the voltage output changes of the applied cell and its adjacent cell, respectively. Our tactile sensor is capable of providing better contrast of tactile images than was previously reported using the tactile sensor with passive-type circuitry, of which crosstalk isolation is calculated to be only half of our values (<23 dB) due to the leak currents in the circuit.^{8,21,22} Furthermore, the low off-current (<0.05 nA) of Si-based TFTs leads to lower power consumption than that of the tactile sensor of passive matrix type whose off-current reaches to as much as 85 nA.⁷

Fig. 4(c) clearly shows a three-dimensional pressure map indicating that contact was made at two spots on the sensor. Compared to the pressure map in Fig. 4(b) obtained when only localized pressure was applied to each tactile cell, the pressure map in Fig. 4(c) includes both the positive and negative voltage outputs, which means that compressive and tensile strains coexist in the sensor array. Since the tactile sensor is attached on the human finger, its response is much related to the mechanical characteristics of the human skin that undergoes both the compressive and the tensile strains according to the type of the physical contact.²³ The high sensitivity of the silicon strain gauges and the high switching speed of the transistor enable tracking the position of a stylus tip moving fast on the tactile sensor, as shown in Fig. 4(d).

This paper explored the prototype tactile sensor employing an 8×8 array of Si strain gauges and their corresponding switches made of single-crystalline Si transistors integrated in an area of smaller than 10 mm^2 that corresponds to the area of the human fingertip. Significant advantages of our Si-based tactile sensor are good performances in terms of repeatability, hysteresis, linearity, and sensitivity originated from the characteristics of Si-semiconductor strain gauges along with the high scanning speed, low crosstalk, and low power consumption resulting from the active-matrix circuitry based on fast speed single-crystalline Si transistor. We expect that these features enable our device to be used in the various applications of emerging fields, such as robot mechatronics for the sophisticated pressure measurements as well as medical instruments.

This work was supported by the Research Program (2012R1A2A1A03006049 and Global Frontier Research

Center for Advanced Soft Electronics: 2013M3A6A5073170) through the National Research Foundation of Korea (NRF), funded by the Ministry of Science, ICT and Future Planning, and the ICT R&D Program (Grant No. 10041066) funded by the Institute for Information & Communication Technology Promotion, Korea.

- ¹M. L. Hammock, A. Chortos, B. C. K. Tee, J. B. H. Tok, and Z. Bao, *Adv. Mater.* **25**, 5997 (2013).
- ²N. Lu and D. H. Kim, *SoRo* **1**, 53 (2014).
- ³T. Sekitani and T. Someya, *Adv. Mater.* **22**, 2228 (2010).
- ⁴C. Ashruf, *Sens. Rev.* **22**, 322 (2002).
- ⁵R. S. Dahiya and M. Valle, *Robotics* (Intech, Croatia, 2008), pp. 289–305.
- ⁶J. Kim, T. N. Ng, and W. S. Kim, *Appl. Phys. Lett.* **101**, 103308 (2012).
- ⁷S. M. Won, H. S. Kim, N. Lu, D. G. Kim, C. Del Solar, T. Duenas, A. Ameen, and J. A. Rogers, *IEEE Trans. Electron Devices* **58**, 4074 (2011).
- ⁸M. Ying, A. P. Bonifas, N. Lu, Y. Su, R. Li, H. Cheng, A. Ameen, Y. Huang, and J. A. Rogers, *Nanotechnology* **23**, 344004 (2012).
- ⁹H. Zhou, J. H. Seo, D. M. Paskiewicz, Y. Zhu, G. K. Celler, P. M. Voyles, W. Zhou, M. G. Lagally, and Z. Ma, *Sci. Rep.* **3**, 1291 (2013).
- ¹⁰D. H. Kim, J. H. Ahn, H. S. Kim, K. J. Lee, T. H. Kim, C. J. Yu, R. G. Nuzzo, and J. A. Rogers, *IEEE Electron Device Lett.* **29**, 73 (2008).
- ¹¹L. Sun, G. Qin, J. H. Seo, G. K. Celler, W. Zhou, and Z. Ma, *Small* **6**, 2553 (2010).
- ¹²J. H. Ahn, H. S. Kim, K. J. Lee, Z. Zhu, E. Menard, R. G. Nuzzo, and J. A. Rogers, *IEEE Electron Device Lett.* **27**, 460 (2006).
- ¹³Q. Cao, H. S. Kim, N. Pimparkar, J. P. Kulkarni, C. Wang, M. Shim, K. Roy, M. A. Alam, and J. A. Rogers, *Nature* **454**, 495 (2008).
- ¹⁴Y. Yuan, G. Giri, A. L. Ayzner, A. P. Zoombelt, S. C. B. Mannsfeld, J. Chen, D. Nordlund, M. F. Toney, J. Huang, and Z. Bao, *Nat. Commun.* **5**, 3005 (2014).
- ¹⁵V. Maheshwari and R. Saraf, *Angew. Chem., Int. Ed.* **47**, 7808 (2008).
- ¹⁶H. Yousef, M. Boukallel, and K. Althoefer, *Sens. Actuators* **167**, 171 (2011).
- ¹⁷M. Kaltenbrunner, T. Sekitani, J. Reeder, T. Yokota, K. Kuribara, T. Tokuhara, M. Drack, R. Schwödianer, I. Graz, S. Bauer-Gogonea, S. Bauer, and T. Someya, *Nature* **499**, 458 (2013).
- ¹⁸C. Wang, D. Hwang, Z. Yu, K. Takei, J. Park, T. Chen, B. Ma, and A. Javey, *Nat. Mater.* **12**, 899 (2013).
- ¹⁹Y. Kanda, *IEEE Trans. Electron Devices* **29**, 64 (1982).
- ²⁰E. S. Dellon, R. Mourey, and A. L. Dellon, *Plast. Reconstr. Surg.* **90**, 112 (1992).
- ²¹W. Hu, X. Niu, R. Zhao, and Q. Pei, *Appl. Phys. Lett.* **102**, 083303 (2013).
- ²²C. Metzger, E. Fleisch, J. Meyer, M. Dansachmüller, I. Graz, M. Kaltenbrunner, C. Keplinger, R. Schwödianer, and S. Bauer, *Appl. Phys. Lett.* **92**, 013506 (2008).
- ²³M. S. Kim, H. J. Shin, and Y. K. Park, *Int. J. Precis. Eng. Manuf.* **13**, 1941 (2012).
- ²⁴See supplementary material at <http://dx.doi.org/10.1063/1.4906373> for detailed figures of optical image, electrical, and mechanical simulation data.